Pentagonal-bipyramidal Dysprosium(III) complexes with two apical phosphine oxide ligands and equatorial pentadentate N_3O_2 Schiff-base ligands: Breakdown of the apical magnetic axiality by strong equatorial crystal field

Tamara A. Bazhenova,[a] Vyacheslav A. Kopotkov,[a] Denis V. Korchagin,[a] Elena A. Yureva,[a] Mikhail V. Zhidkov,[a] Alexei I. Dmitriev,[a] Ilya A. Yakushev,[b] Nikolay N. Efimov,[b] Konstantin A. Babeshkin,[b] Vladimir S. Mironov*[c] and Eduard B. Yagubskii*[a]

[a.] *Federal Research Centre of Problems of Chemical Physics and Medicinal Chemistry, FRC PCP MC RAS, 1 Academician Semenov av., Chernogolovka, 142432, Russian Federation. E-mail: yagubski@gmail.com*
[b.] *Kurnakov Institute of General and Inorganic Chemistry, IGIC RAS, 31 Leninskii av., Moscow, 119071, Russian Federation.*
[c.] *National Research Center "Kurchatov Institute", 1 Academician Kurchatov sq., Moscow, 123182, Russian Federation. E-mail: mirsa@list.ru*

Table of Contents:

Figure S1. Crystal-field splitting patterns of Dy^{3+} ion arising from (a) apical ligands, (b) equatorial ligands of a pentagonal-bipyramidal Dy complex

Figure S2. Infrared spectrum of the complex $[Dy(L^{CH3})(Cy_3PO)_2]ClO_4{\cdot}CH_3CN$ **(1)**

Figure S3. Infrared spectrum of the complex **[**$Dy(L^{2(t\text{-}Bu)})(Ph_3PO)_2]ClO4{\cdot}C_2H_5OH$ **(2)**

Table S1 Crystal Data and Structure Refinement for **1-3**

Figure S5. Powder X-ray diffraction of the complex $[Dy(L^{CH3})(Cy_3PO)_2]ClO_4{\cdot}CH_3CN$ (**1**)

Figure S6. Powder X-ray diffraction of the complex $[Dy(L^{2(t\text{-}Bu)})(Ph_3PO)_2]ClO_4{\cdot}0.63C_2H_5OH$ (**2**)

Figure S7. Powder X-ray diffraction of the complex $[Dy(L^{OCH3})(Ph_3PO)_2]ClO_4{\cdot}2H_2O$ (**3**)

Figure S8. **^{1}H NMR and ^{13}C NMR** spectra of 3,5 di-*tert*-butylbenzoic acid hydrazide

Figure S9. ^{1}H NMR spectrum for compound $\mathbf{H_2L^{OCH3}}$

Figure S10. **^{13}C NMR** spectrum for compound $\mathbf{H_2L^{OCH3}}$

Table S2 The local symmetry of Dy(III) ions for **1**–**3** defined by the continuous shape measure (CShM) analysis with SHAPE software

Table S3 Main angles for complex **1**

Table S4 Main angles for complex **2**

Table S5 Main angles for complex **3**

Figure S11. π-stacking interaction in structure **3**

Figure S12. Hysteresis loops at different magnetic field sweep rates (50 Oe/s and 150 Oe/s) at temperature 2 K in structure **3**.

Figure S13. Hysteresis loops at different temperatures 2 K, 3 K and 5 K and magnetic field sweep rates 50 Oe/s (a) and 150 Oe/s (b) in structure **3**.

Figure S14. Frequency dependences of the in-phase ac susceptibility (left panel) and Cole−Cole plots (right panel) for complexes **1–3** at zero dc field and stated temperatures

Table S6 Best fit parameters for **1** at zero dc field

Table S7 Best fit parameters for **2** at zero dc field

Table S8 Best fit parameters for **3** at zero dc field

Figure S15. Natural log of the relaxation times τ_1 and τ_2 vs the inverse temperature for **1** (a) and **2** (b) at zero dc field

Figure S16. Frequency dependences of the in-phase (a) and out-of-phase (b) ac susceptibility, Cole−Cole plots (c) for **1** at 10 K and indicated dc fields

Table S9 Best fit parameters for **1** at 10 K

Figure S17. Frequency dependences of the in-phase (a) and out-of-phase (b) ac susceptibility; (c) Cole−Cole plots for **2** at 8 K and indicated dc fields; (d) field dependence of the relaxation time τ at 8 K

Table S10 Best fit parameters for **2** at 8 K

Figure S18. Frequency dependences of the out-of-phase (a) ac susceptibility; (b) field dependence of the relaxation time τ for **3** at 10 K

Table S11 Best fit parameters for **3** at 10 K (R^2 = 0.99798)

Figure S19. Frequency dependences of the in-phase ac susceptibility (left panel) and Cole−Cole plots (right panel) for complexes **1–3** at dc field 1000 Oe and stated temperatures

Table S12 Best fit parameters for **1** at dc field 1000 Oe

Table S13 Best fit parameters for **2** at dc field 1000 Oe

Table S14 Best fit parameters for **3** at dc field 1000 Oe

Figure S20. The inverse temperature dependences of the relaxation time τ for **2** (a) and **3** (b) at zero dc field (black lines) and 1000 Oe (red lines)

Table S15 The *ab initio* computed energy levels (cm^{-1}) with g-tensors of the eight lowest KDs for two crystallographic non-equivalent complexes in **1** and **2**

Table S16 SINGLE_ANISO computed wave function decomposition analysis for lowest KDs of Dy(III) ions for two crystallographic non-equivalent complexes in **1** and **2**

Figure S21. The molecular structures of **1** (a), **2** (b) and **3** (c) together with the easy axes (magenta) of ground KD obtained within the *ab initio* SA-CASSCF/RASSI-SO/SINGLE_ANISO calculation

Figure S22. Computed possible magnetization relaxation pathways for **1** (a), **2** (b) and **3** (c)

Table S17 The *ab initio* computed CF parameter of complexes **1-3**

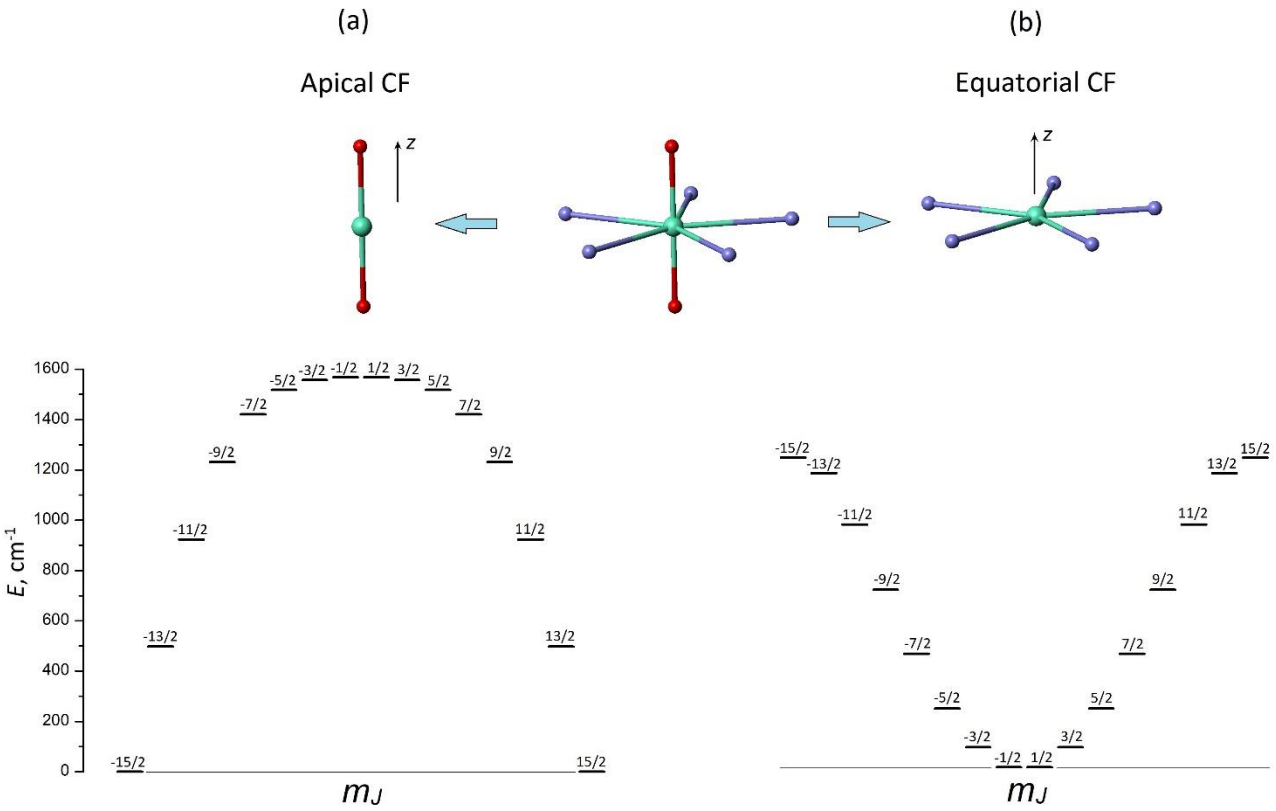

Figure S1. Crystal-field splitting patterns of Dy^{3+} ion arising from (a) apical ligands, (b) equatorial ligands of a pentagonal-bipyramidal Dy complex.

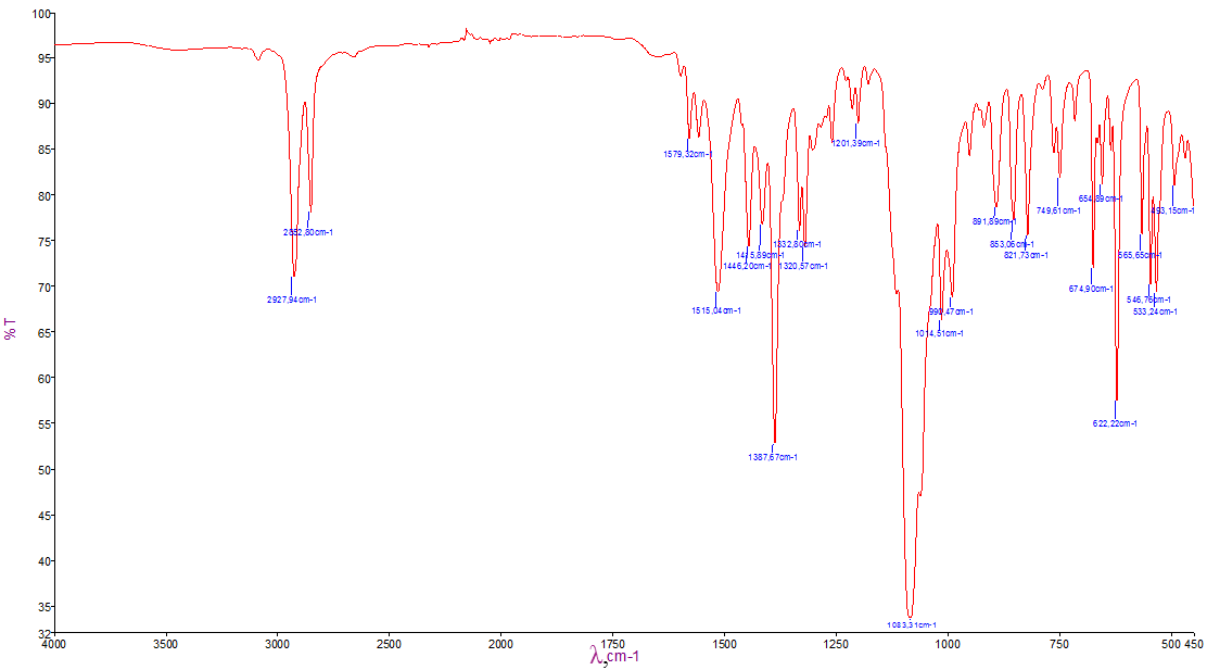

Figure S2. Infrared spectrum of the complex $[Dy(L^{CH3})(Cy_3PO)_2]ClO_4{\cdot}CH_3CN$ (**1**)**.**

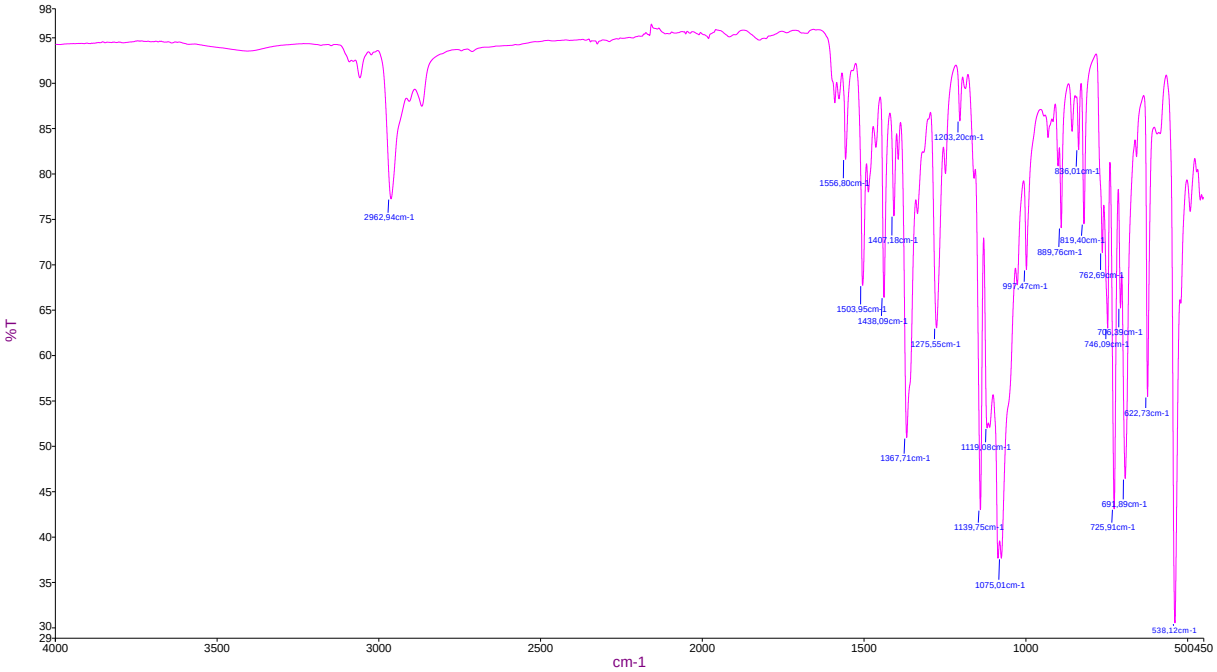

Figure S3. Infrared spectrum of the complex **[**$Dy(L^{2(t\text{-}Bu)})(Ph_3PO)_2]ClO4\cdot C_2H_5OH$ (**2**)**.**

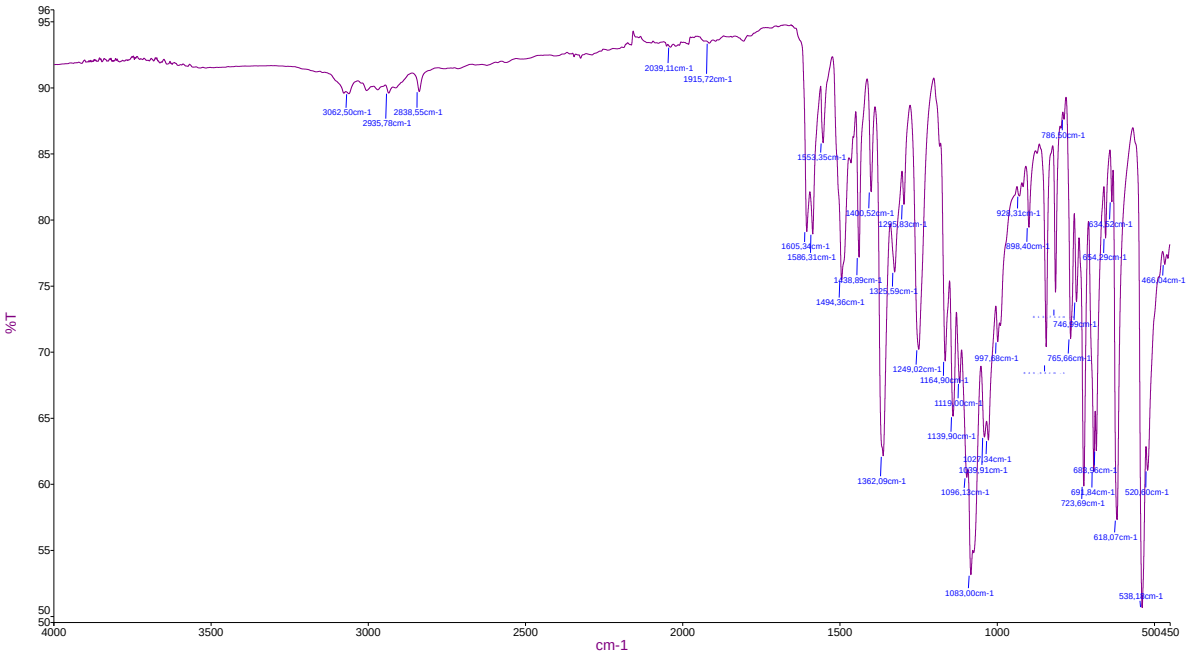

Figure S4. Infrared spectrum of the complex **[**$Dy(L^{OCH3})(Ph_3PO)_2]ClO_4\cdot 2H_2O$ (**3**).

Table S1 Crystal Data and Structure Refinement for **1-3**

Identification code	**1**	**2**	**3**
CCDC No	2239615	2239616	2239617
Empirical formula	$C_{51}H_{84}ClDyN_6O_8P_2$	$C_{76.268}H_{84.804}ClDyN_5O_{8.634}P_2$	$C_{61}H_{57}ClDyN_5O_{12}P_2$
Formula weight	1169.13	1469.53	1312.00
Color	yellow	yellow	yellow
Temperature, K	100(2)	150	100(2)
Crystal size, mm	0.420×0.330×0.190	0.38×0.21×0.12	0.240×0.180×0.100
Wavelength, Å	0.71073	0.71073	0.71073
Crystal system	Monoclinic	Monoclinic	Triclinic
Space group	$P2_1/n$	$P2_1/c$	P-1
a, Å	25.7341(6)	22.8749(7)	12.2689(5)
b, Å	16.5737(3)	28.3369(8)	13.1736(6)
c, Å	26.5177(5)	22.9566(7)	19.6615(9)
α, deg.	90	90	99.0068(16)
β, deg.	101.6240(10)	98.4170(10)	93.1825(17)
γ, deg.	90	90	113.5421(15)
V, Å^3	11078.1(4)	14720.3(8)	2852.8(2)
Z	8	8	2
Density (calc.), Mg/m^3	1.402	1.326	1.527
μ, mm^{-1}	1.510	1.153	1.481
F(000)	4872	6075.9	1334
Theta range, deg.	1.588 – 30.596	1.376 – 29.987	1.826 – 25.350
Index ranges	−36 ≤ h ≤ 36, −23 ≤ k ≤ 23, −37 ≤ l ≤ 37	−32 ≤ h ≤ 32, −39 ≤ k ≤ 39, −32 ≤ l ≤ 32	−14 ≤ h ≤ 14, −15 ≤ k ≤ 15, −23 ≤ l ≤ 23
Reflections collected	172464	242798	38607
Independent reflections	33918 (R_{int} = 0.0386)	42864 (R_{int} = 0.0612)	10442 (R_{int} = 0.0447)
Reflections observed	33918	42864	10442
Data / restraints / parameters	33918 / 0 / 1253	42864 / 742 / 1994	10442 / 216 / 831
R_1 / wR_2 (I > 2σ(I))	R_1 = 0.0273, wR_2 = 0.0590	R_1 = 0.0371, wR_2 = 0.0760	R_1 = 0.0386, wR_2 = 0.0814
R_1 / wR_2 (all data)	R_1 = 0.0424, wR_2 = 0.0641	R_1 = 0.0623, wR_2 = 0.0841	R_1 = 0.0439, wR_2 = 0.0834
Goodness-of-fit on F^2	1.013	1.015	1.091
T_{min} / T_{max}	0.7461 / 0.6330	0.1182 / 0.0814	0.2125 / 0.1704
$\Delta\rho_{max}$ / $\Delta\rho_{min}$, e·Å^{-3}	−0.787 / 0.601	−0.915 / 0.675	−1.301 / 1.640

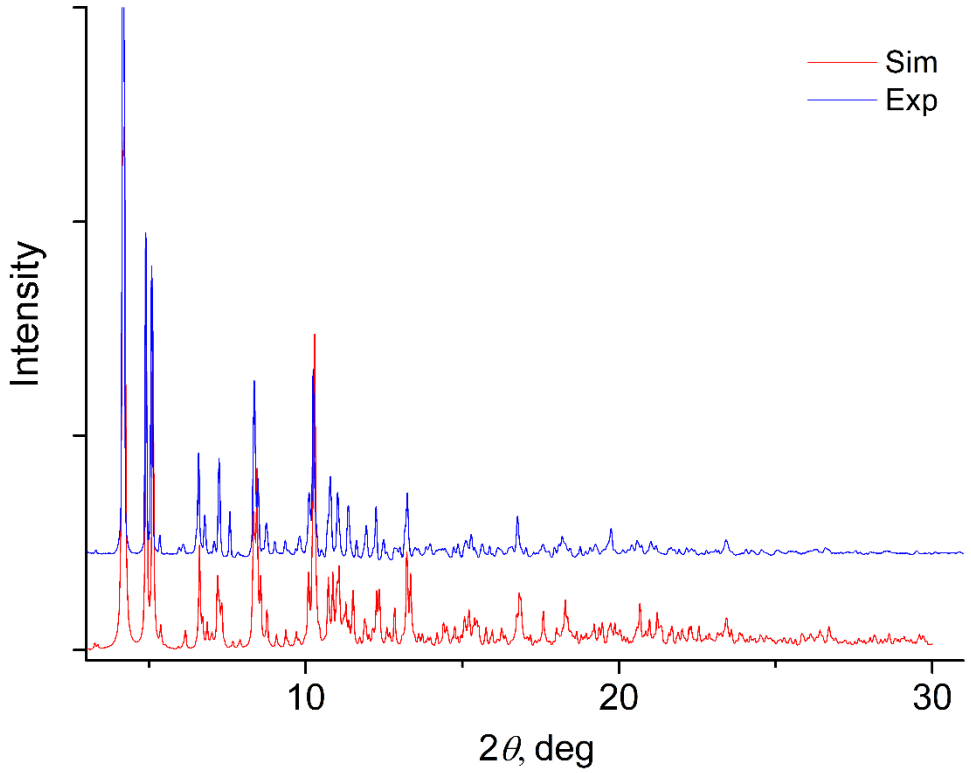

Figure S5. Powder X-ray diffraction of the complex [Dy(L^{CH3})($Cy_3PO)_2$]ClO_4·CH_3CN (**1**).

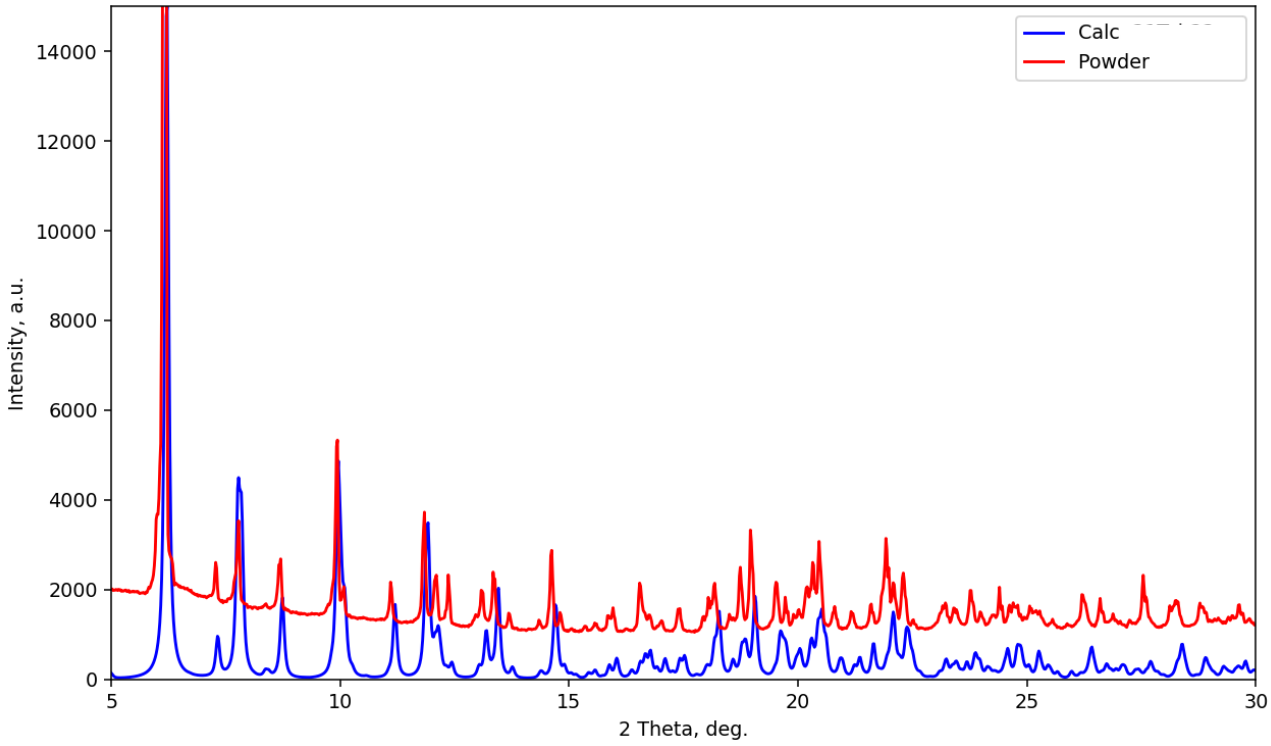

Figure S6. Powder X-ray diffraction of the complex [Dy($L^{2(t\text{-}Bu)}$)($Ph_3PO)_2$]ClO_4·$0.63C_2H_5OH$ (**2**).

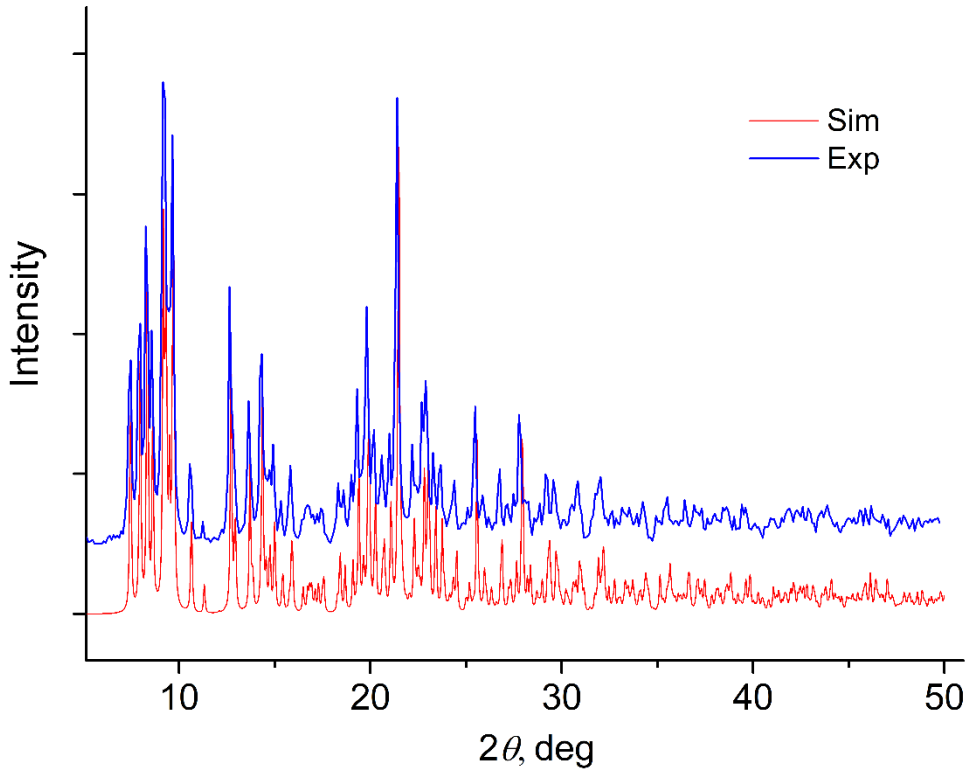

Figure S7. Powder X-ray diffraction of the complex $[Dy(L^{OCH3})(Ph_3PO)_2]ClO_4 \cdot 2H_2O$ (**3**)

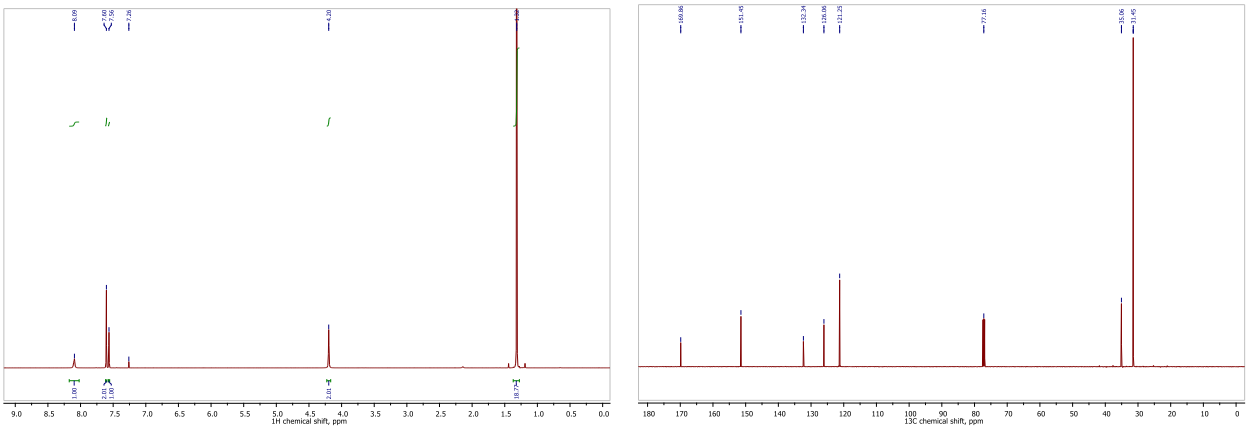

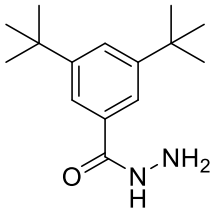	^{1}H NMR ($CDCl_3$, 500 MHz): 8.09 (1H, s, NH), 7.60 (2H, m), 7.56 (1H, m), 4.20 (2H, s, NH_2), 1.32 (18H, s, $C(CH_3)_3$). ^{13}C NMR ($CDCl_3$, 126 MHz): 169.86, 151.45, 132.34, 126.06, 121.25, 35.06, 31.45.

Figure S8. **^{1}H NMR and ^{13}C NMR** spectra of 3,5 di-*tert*-butylbenzoic acid hydrazide (solvent – $CDCl_3$).

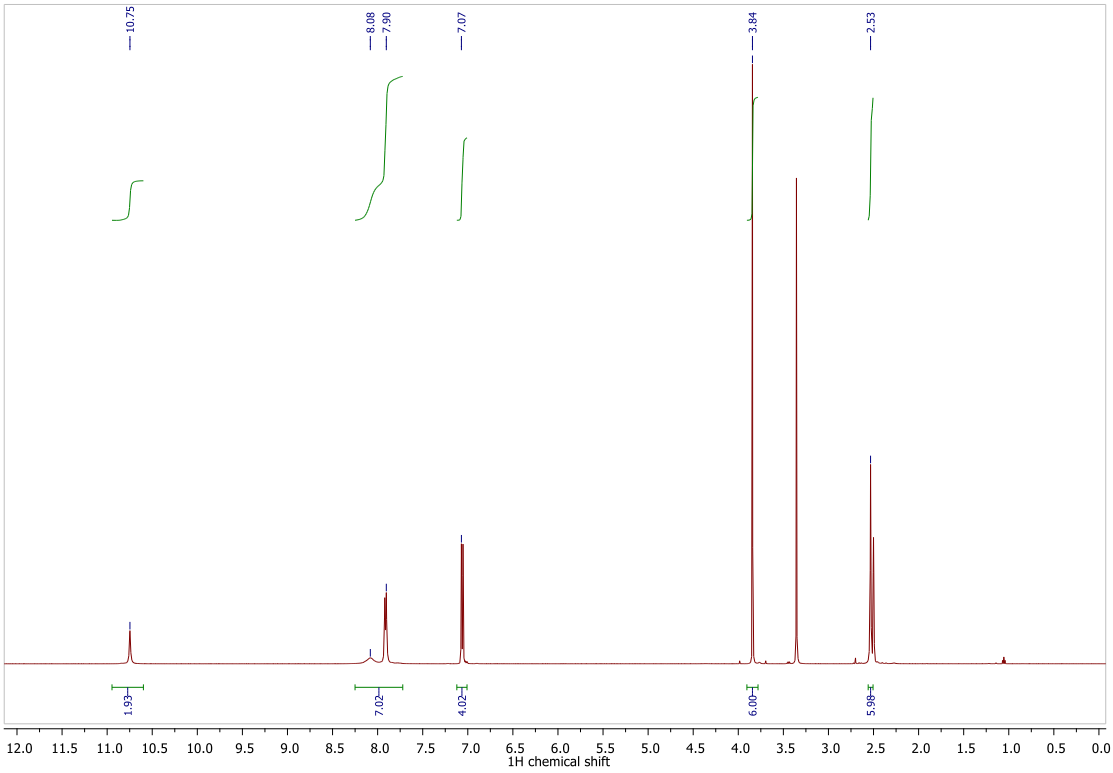

Figure S9. **^{1}H NMR** spectrum for compound **H_2L^{OCH3}** (DMSO-D6, 500 МГц), δ: *10.75 (2H, s, NH), 8.35-7.54 (3H, m), 7.90 (4H, d), 7.07 (4H, d), 3.84 (6H, s, OCH_3), 2.53 (6H, s, CH_3).*

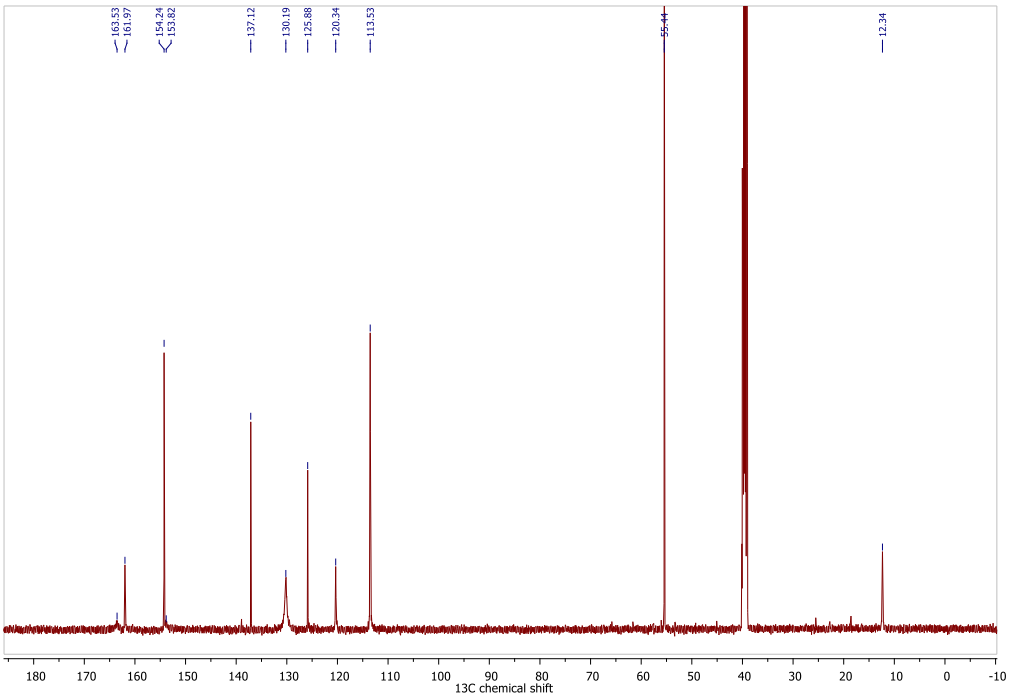

Figure S10. **^{13}C NMR** spectrum for compound **H_2L^{OCH3}** (DMSO-D6, 126 MHz), δ: *163.53, 161.97, 154.24, 153.82, 137.12, 130.19, 125.88, 120.34, 113.53, 55.44, 12.34.*

Table S2 The local symmetry of Dy(III) ions for **1**–**3** defined by the continuous shape measure (CShM) analysis with SHAPE software

№	Polyhedron	Symmetry	**1a**	**1b**	**2a**	**2b**	**3**
1	Heptagon	D_{7h}	32.064	32.608	32.208	32.587	31.961
2	Hexagonal pyramid	C_{6v}	22.083	22.098	20.488	22.255	21.292
3	**Pentagonal bipyramid**	$\mathbf{D_{5h}}$	**1.202**	**1.154**	**1.569**	**1.450**	**1.377**
4	Capped octahedron	C_{3v}	8.111	8.271	7.927	8.247	8.064
5	Capped trigonal prism	C_{2v}	6.336	6.708	6.414	6.624	6.356
6	Johnson pentagonal bipyramid J13	D_{5h}	3.909	3.893	4.339	4.142	4.298
7	Johnson elongated triangular pyramid J7	C_{3v}	21.717	21.931	20.177	20.416	19.991

Table S3 Main angles for complex **1**

Bonds	Angles, °	Bonds	Angles, °
O(1)–Dy(1)–O(2)	99.62(4)	O(1A)–Dy(2)–N(2A)	65.40(4)
O(1)–Dy(1)–N(2)	65.04(4)	O(1A)–Dy(2)–N(3A)	130.64(4)
O(1)–Dy(1)–N(3)	129.77(4)	O(1A)–Dy(2)–N(4A)	164.36(5)
O(1)–Dy(1)–N(4)	164.98(4)	O(2A)–Dy(2)–O(1A)	99.40(4)
O(2)–Dy(1)–N(2)	164.65(4)	O(2A)–Dy(2)–N(2A)	164.76(4)
O(2)–Dy(1)–N(3)	130.53(4)	O(2A)–Dy(2)–N(3A)	129.95(4)
O(2)–Dy(1)–N(4)	65.43(4)	O(2A)–Dy(2)–N(4A)	64.97(4)
O(3)–Dy(1)–O(1)	93.38(4)	O(3A)–Dy(2)–O(1A)	92.00(4)
O(3)–Dy(1)–O(2)	91.98(4)	O(3A)–Dy(2)–O(2A)	92.34(4)
O(3)–Dy(1)–N(2)	89.68(4)	O(3A)–Dy(2)–N(2A)	87.34(4)
O(3)–Dy(1)–N(3)	83.59(4)	O(3A)–Dy(2)–N(3A)	85.93(4)
O(3)–Dy(1)–N(4)	85.94(4)	O(3A)–Dy(2)–N(4A)	88.22(4)
O(4)–Dy(1)–O(1)	93.73(4)	O(4A)–Dy(2)–O(1A)	93.59(4)
O(4)–Dy(1)–O(2)	92.41(4)	O(4A)–Dy(2)–O(2A)	93.08(4)
O(4)–Dy(1)–O(3)	170.91(4)	O(4A)–Dy(2)–O(3A)	171.49(4)
O(4)–Dy(1)–N(2)	88.18(4)	O(4A)–Dy(2)–N(2A)	89.14(4)
O(4)–Dy(1)–N(3)	87.51(4)	O(4A)–Dy(2)–N(3A)	85.56(4)
O(4)–Dy(1)–N(4)	88.66(4)	O(4A)–Dy(2)–N(4A)	88.14(4)
N(2)–Dy(1)–N(3)	64.82(4)	N(2A)–Dy(2)–N(3A)	65.24(5)
N(4)–Dy(1)–N(2)	129.91(4)	N(2A)–Dy(2)–N(4A)	130.21(5)
N(4)–Dy(1)–N(3)	65.11(4)	N(3A)–Dy(2)–N(4A)	64.98(5)

Table S4 Main angles for complex **2**.

Bonds	Angles, °	Bonds	Angles, °
O(1)–Dy(1)–N(2)	65.34(6)	O(1A)–Dy(2)–O(2A)	101.52(5)
O(1)–Dy(1)–N(3)	129.65(6)	O(1A)–Dy(2)–N(2A)	64.79(6)
O(1)–Dy(1)–N(4)	166.12(7)	O(1A)–Dy(2)–N(3A)	128.82(6)
O(2)–Dy(1)–O(1)	101.12(6)	O(1A)–Dy(2)–N(4A)	165.17(6)
O(2)–Dy(1)–N(2)	164.77(7)	O(2A)–Dy(2)–N(2A)	165.09(6)
O(2)–Dy(1)–N(3)	129.08(7)	O(2A)–Dy(2)–N(3A)	129.67(6)
O(2)–Dy(1)–N(4)	65.17(7)	O(2A)–Dy(2)–N(4A)	65.08(6)
O(3)–Dy(1)–O(1)	93.08(6)	O(3A)–Dy(2)–O(1A)	97.08(6)
O(3)–Dy(1)–O(2)	87.46(6)	O(3A)–Dy(2)–O(2A)	89.28(6)
O(3)–Dy(1)–O(4)	176.71(6)	O(3A)–Dy(2)–O(4A)	169.96(6)
O(3)–Dy(1)–N(2)	86.41(7)	O(3A)–Dy(2)–N(2A)	86.77(6)
O(3)–Dy(1)–N(3)	86.39(7)	O(3A)–Dy(2)–N(3A)	85.03(6)
O(3)–Dy(1)–N(4)	88.58(7)	O(3A)–Dy(2)–N(4A)	89.36(6)
O(4)–Dy(1)–O(1)	87.34(6)	O(4A)–Dy(2)–O(1A)	90.40(6)
O(4)–Dy(1)–O(2)	95.67(6)	O(4A)–Dy(2)–O(2A)	95.81(6)
O(4)–Dy(1)–N(2)	90.80(7)	O(4A)–Dy(2)–N(2A)	90.39(6)
O(4)–Dy(1)–N(3)	90.82(7)	O(4A)–Dy(2)–N(3A)	85.06(6)
O(4)–Dy(1)–N(4)	91.80(7)	O(4A)–Dy(2)–N(4A)	84.97(6)
N(2)–Dy(1)–N(3)	64.38(7)	N(3A)–Dy(2)–N(2A)	64.29(6)
N(2)–Dy(1)–N(4)	128.53(7)	N(4A)–Dy(2)–N(2A)	129.18(6)
N(4)–Dy(1)–N(3)	64.19(7)	N(4A)–Dy(2)–N(3A)	64.89(6)

Table S5 Main angles for complex **3**

Bonds	Angles, °	Bonds	Angles, °
O(1)–Dy(1)–N(2)	65.05(10)	O(5)–Dy(1)–N(4)	87.94(10)
O(1)–Dy(1)–N(3)	130.10(10)	O(6)–Dy(1)–O(1)	91.18(9)
O(1)–Dy(1)–N(4)	164.61(10)	O(6)–Dy(1)–O(2)	88.00(10)
O(2)–Dy(1)–O(1)	99.48(9)	O(6)–Dy(1)–O(5)	174.43(10)
O(2)–Dy(1)–O(5)	91.97(10)	O(6)–Dy(1)–N(2)	85.13(11)
O(2)–Dy(1)–N(2)	162.86(10)	O(6)–Dy(1)–N(3)	83.25(11)
O(2)–Dy(1)–N(3)	129.62(10)	O(6)–Dy(1)–N(4)	86.99(10)
O(2)–Dy(1)–N(4)	65.21(10)	N(2)–Dy(1)–N(3)	65.07(11)
O(5)–Dy(1)–O(1)	94.32(9)	N(2)–Dy(1)–N(4)	129.87(11)
O(5)–Dy(1)–N(2)	96.38(11)	N(3)–Dy(1)–N(4)	64.86(11)
O(5)–Dy(1)–N(3)	92.51(11)		

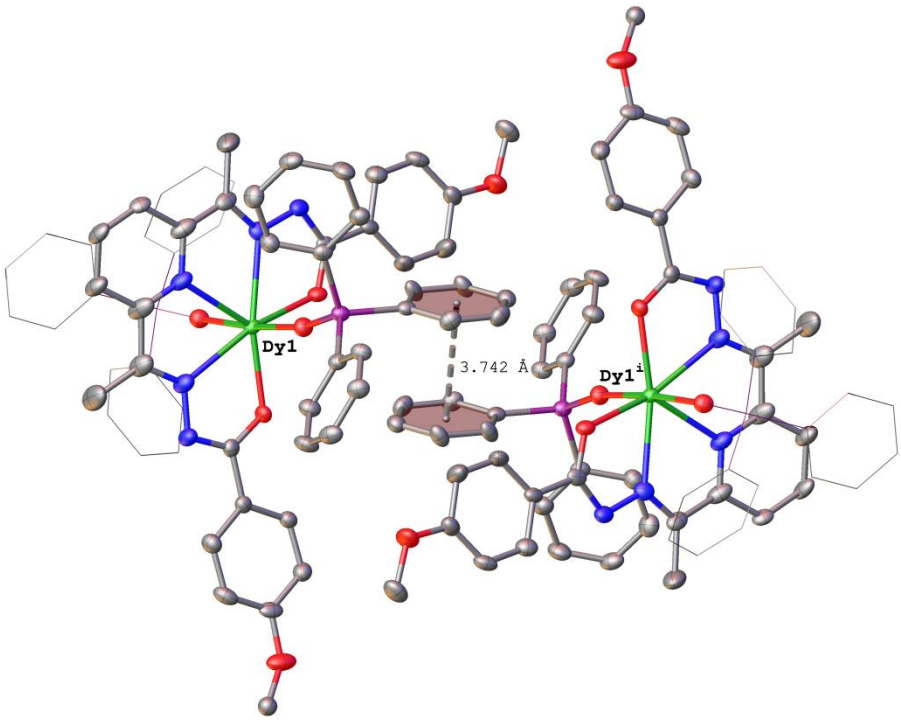

Figure S11. π-stacking interaction in structure **3**.

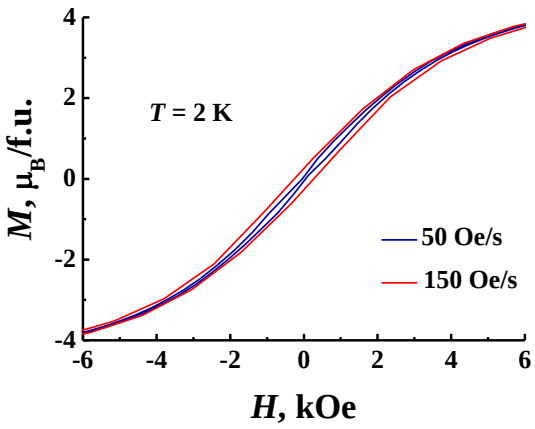

Figure S12. Hysteresis loops at different magnetic field sweep rates (50 Oe/s and 150 Oe/s) at temperature 2 K in structure **3**.

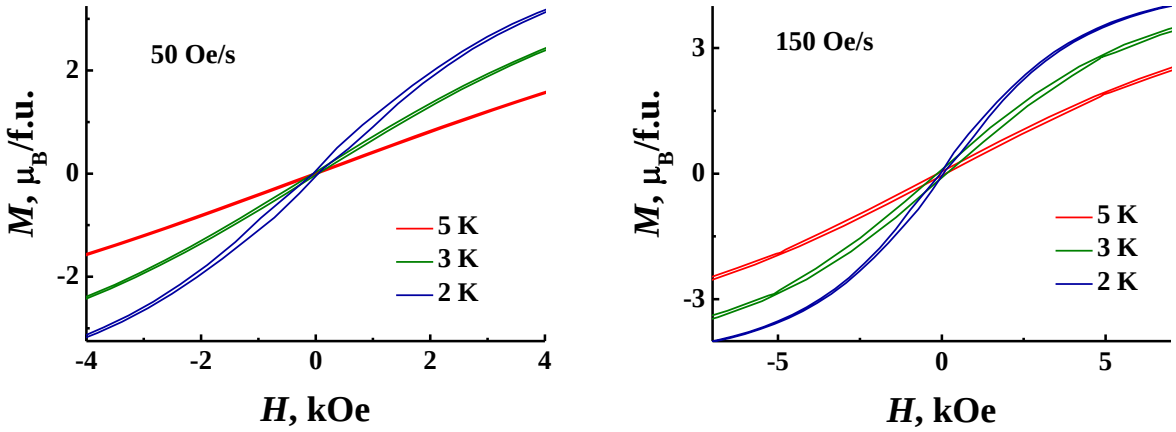

Figure S13. Hysteresis loops at different temperatures 2 K, 3 K and 5 K and magnetic field sweep rates 50 Oe/s (a) and 150 Oe/s (b) in structure **3**.

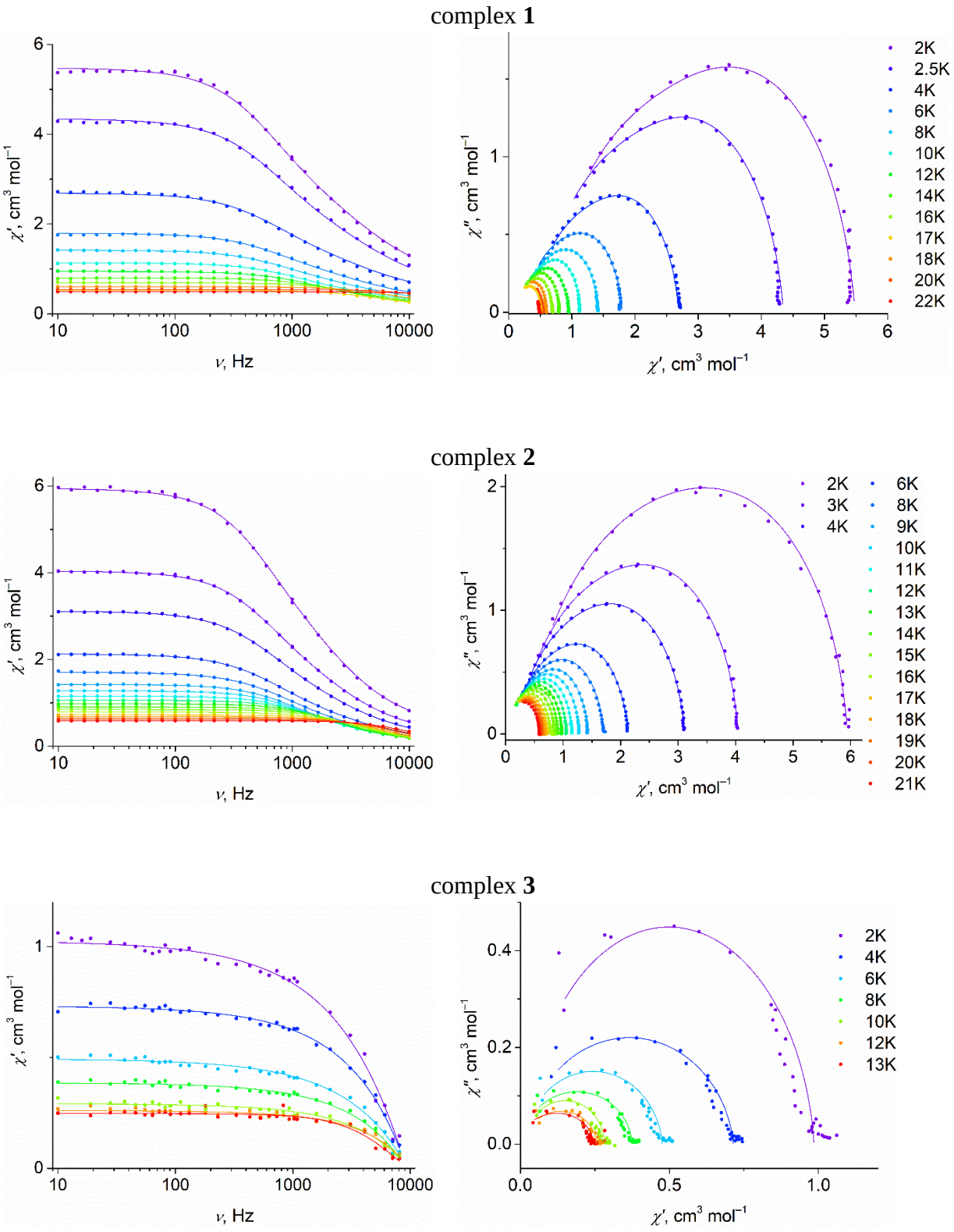

Figure S14. Frequency dependences of the in-phase ac susceptibility (left panel) and Cole−Cole plots (right panel) for complexes **1–3** at zero dc field and stated temperatures. Dots are experimental data; solid lines indicate fit data with parameters listed in Tables S6–S8.

Table S6 Best fit parameters for **1** at zero dc field (R^2 = 0.99978)*

T, K	χ_S, $cm^3\ mol^{-1}$	$\Delta\chi_{T1}$, $cm^3\ mol^{-1}$	τ_1, s	α_1	$\Delta\chi_{T2}$, $cm^3\ mol^{-1}$	τ_2, s	α_2
2	0.611	2.440	$2.42\cdot10^{-4}$	0.080	2.431	$3.89\cdot10^{-5}$	0.223
2.5	0.490	1.993	$2.30\cdot10^{-4}$	0.087	1.866	$3.71\cdot10^{-5}$	0.217
4	0.385	1.145	$2.28\cdot10^{-4}$	0.082	1.162	$3.82\cdot10^{-5}$	0.223
6	0.254	0.713	$2.10\cdot10^{-4}$	0.075	0.832	$3.93\cdot10^{-5}$	0.217
8	0.235	0.615	$1.84\cdot10^{-4}$	0.078	0.570	$3.60\cdot10^{-5}$	0.202
10	0.164	0.567	$1.42\cdot10^{-4}$	0.069	0.407	$2.42\cdot10^{-5}$	0.223
12	0.140	0.517	$1.06\cdot10^{-4}$	0.069	0.289	$1.62\cdot10^{-5}$	0.222
14	0.114	0.487	$6.89\cdot10^{-5}$	0.070	0.201	$1.04\cdot10^{-5}$	0.206
16	0.131	0.458	$3.99\cdot10^{-5}$	0.071	0.106	$5.27\cdot10^{-6}$	0.174
17	0.139	0.389	$2.63\cdot10^{-5}$	0.082	–	–	–
18	0.178	0.422	$1.96\cdot10^{-5}$	0.047	–	–	–
20	0.177	0.366	$8.65\cdot10^{-6}$	0.042	–	–	–
22	0.204	0.286	$3.72\cdot10^{-6}$	0.083	–	–	–

* at temperatures above17 K, the data were fitted by the generalized Debye model

Table S7 Best fit parameters for **2** at zero dc field (R^2 = 0.99987)

T, K	χ_S, $cm^3\ mol^{-1}$	$\Delta\chi_{T1}$, $cm^3\ mol^{-1}$	τ_1, s	α_1	$\Delta\chi_{T2}$, $cm^3\ mol^{-1}$	τ_2, s	α_2
2	0.350	2.179	$2.843\cdot10^{-4}$	0.032	3.423	$7.460\cdot10^{-5}$	0.2
3	0.222	1.703	$2.650\cdot10^{-4}$	0.038	2.121	$6.623\cdot10^{-5}$	0.2
4	0.164	1.543	$2.468\cdot10^{-4}$	0.067	1.409	$5.799\cdot10^{-5}$	0.2
6	0.108	1.128	$2.272\cdot10^{-4}$	0.070	0.893	$5.222\cdot10^{-5}$	0.2
8	0.087	0.980	$1.868\cdot10^{-4}$	0.070	0.638	$4.620\cdot10^{-5}$	0.2
9	0.061	0.788	$1.639\cdot10^{-4}$	0.027	0.577	$4.065\cdot10^{-5}$	0.2
10	0.057	0.703	$1.381\cdot10^{-4}$	0.015	0.519	$3.926\cdot10^{-5}$	0.2
11	0.049	0.629	$1.149\cdot10^{-4}$	0.007	0.478	$3.656\cdot10^{-5}$	0.2
12	0.025	0.712	$8.900\cdot10^{-5}$	0.018	0.321	$2.036\cdot10^{-5}$	0.2
13	0.032	0.640	$7.461\cdot10^{-5}$	0.008	0.305	$2.131\cdot10^{-5}$	0.2
14	0.002	0.611	$6.264\cdot10^{-5}$	0.001	0.294	$1.453\cdot10^{-5}$	0.2
15	0.006	0.631	$4.934\cdot10^{-5}$	0.016	0.210	$1.034\cdot10^{-5}$	0.2
16	0.001	0.592	$4.176\cdot10^{-5}$	0.046	0.196	$1.068\cdot10^{-5}$	0.2
17	0.001	0.548	$3.417\cdot10^{-5}$	0.022	0.172	$7.965\cdot10^{-6}$	0.2
18	0.001	0.509	$2.865\cdot10^{-5}$	0.012	0.168	$7.067\cdot10^{-6}$	0.2
19	0.001	0.512	$2.317\cdot10^{-5}$	0.016	0.132	$4.864\cdot10^{-6}$	0.2
20	0.001	0.503	$1.926\cdot10^{-5}$	0.018	0.112	$3.147\cdot10^{-6}$	0.2
21	0.001	0.498	$1.536\cdot10^{-5}$	0.020	0.089	$2.276\cdot10^{-6}$	0.2

Table S8 Best fit parameters for **3** at zero dc field (R^2 = 0.99952)

T, K	χ_S, cm^3 mol^{-1}	$\Delta\chi_T$, cm^3 mol^{-1}	τ, s	α
2	0.102	0.998	$4.617\cdot10^{-5}$	0.067
4	0.073	0.493	$4.458\cdot10^{-5}$	0.073
6	0.049	0.327	$4.299\cdot10^{-5}$	0.053
8	0.038	0.234	$4.140\cdot10^{-5}$	0.049
10	0.029	0.182	$3.980\cdot10^{-5}$	0.007
12	0.026	0.134	$3.662\cdot10^{-5}$	0.005
13	0.024	0.128	$3.184\cdot10^{-5}$	0.006

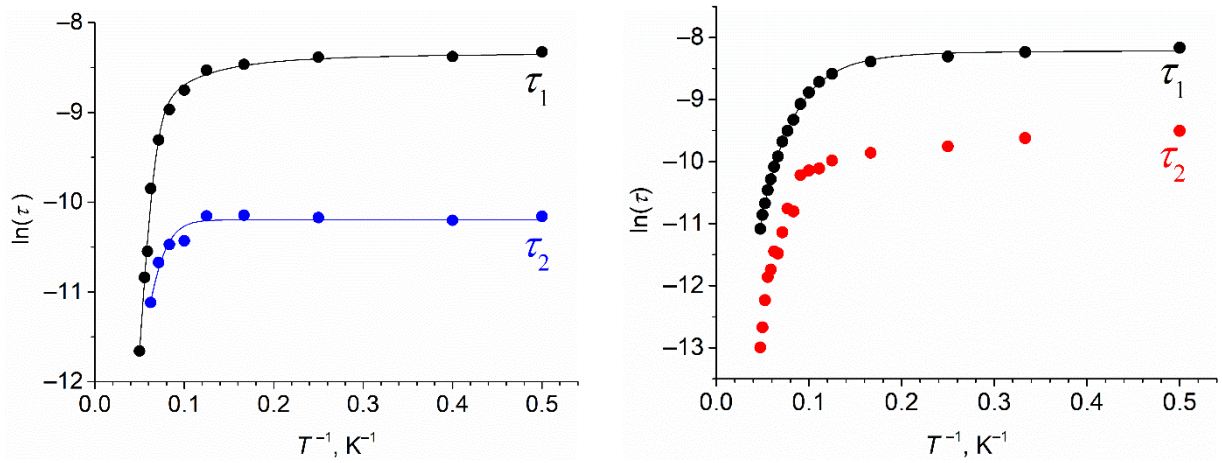

Figure S15. Natural log of the relaxation times τ_1 and τ_2 vs the inverse temperature for **1** (a) and **2** (b) at zero dc field.

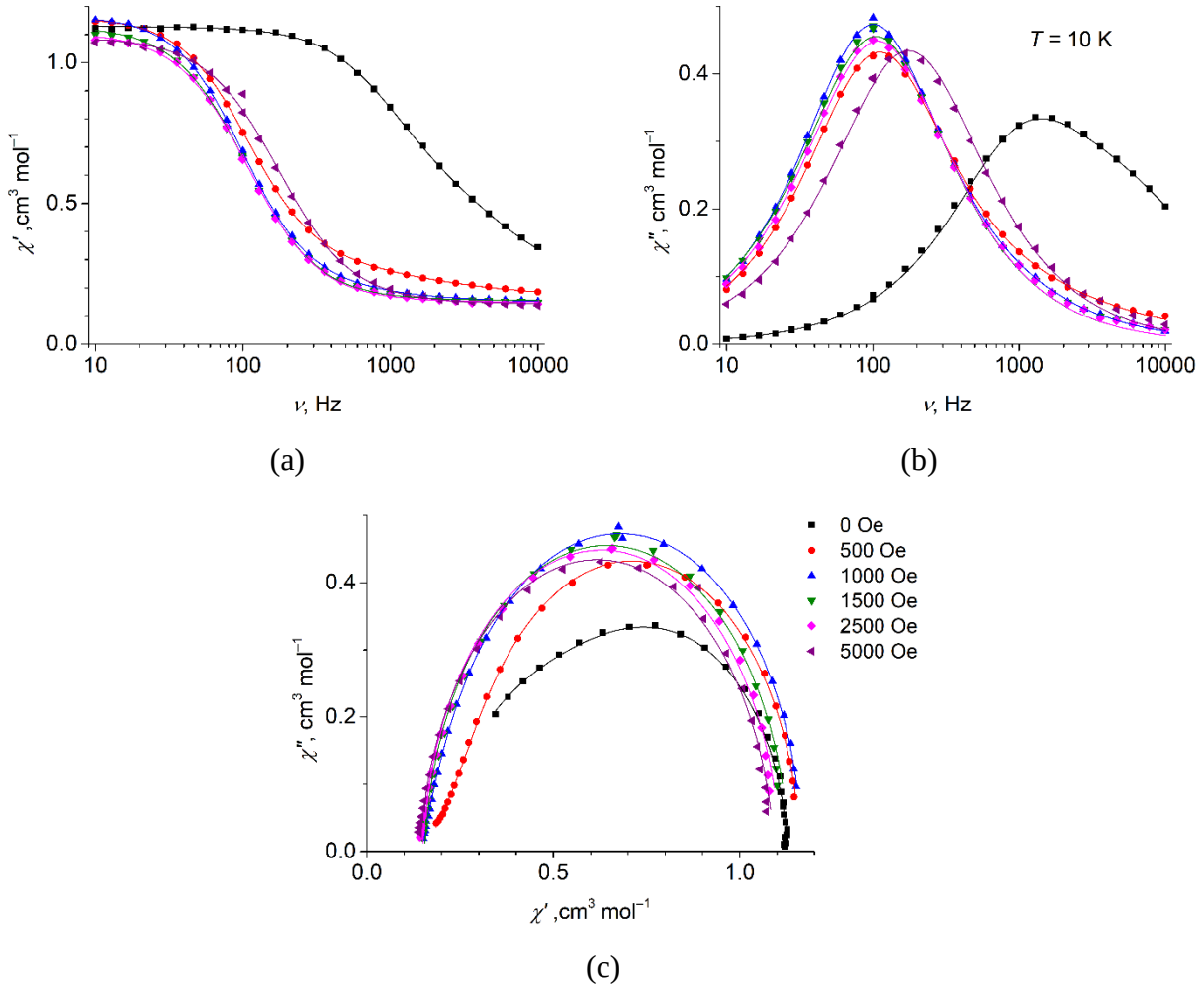

Figure S16. Frequency dependences of the in-phase (a) and out-of-phase (b) ac susceptibility, Cole−Cole plots (c) for **1** at 10 K and indicated dc fields. Symbols are experimental data; solid lines indicate fits.

Table S9 Best fit parameters for **1** at 10 K (R^2 = 0.99972)

H, Oe	χ_S, $cm^3\ mol^{-1}$	$\Delta\chi_{T1}$, $cm^3\ mol^{-1}$	τ_1, s	α_1	$\Delta\chi_{T2}$, $cm^3\ mol^{-1}$	τ_2, s	α_2
0	0.195	0.503	$1.554\cdot10^{-4}$	0.036	0.432	$2.927\cdot10^{-5}$	0.167
500	0.159	0.836	$1.470\cdot10^{-3}$	0.017	0.168	$1.406\cdot10^{-4}$	0.378
1000	0.147	0.916	$1.620\cdot10^{-3}$	0.010	–	–	–
1500	0.155	0.977	$1.520\cdot10^{-3}$	0.045	–	–	–
2500	0.150	0.958	$1.470\cdot10^{-3}$	0.042	–	–	–
5000	0.143	0.949	$9.095\cdot10^{-4}$	0.057	–	–	–

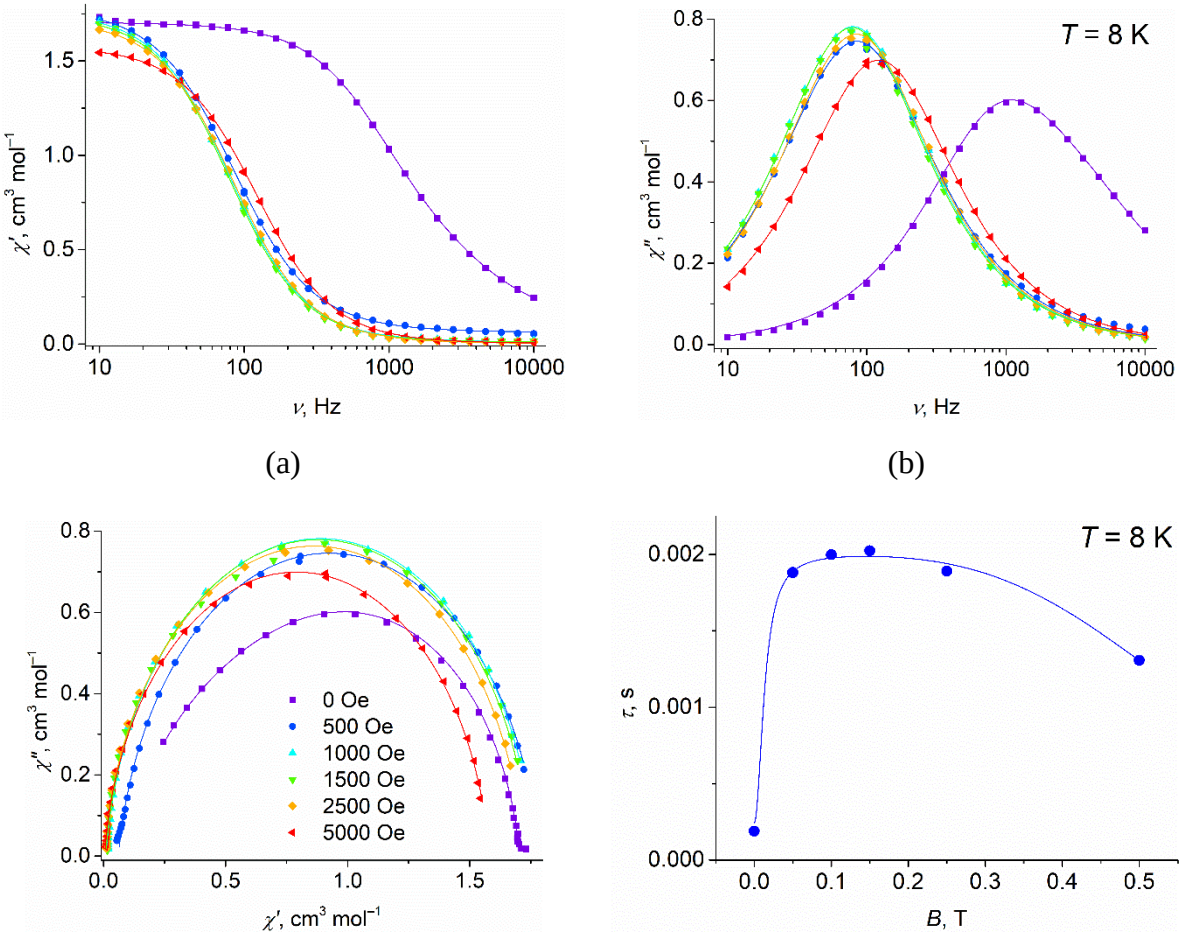

Figure S17. Frequency dependences of the in-phase (a) and out-of-phase (b) ac susceptibility; (c) Cole–Cole plots for **2** at 8 K and indicated dc fields; (d) field dependence of the relaxation time τ at 8 K. Symbols are experimental data; solid lines indicate fits.

Table S10 Best fit parameters for **2** at 8 K (R^2 = 0.99982)

H, Oe	χ_S, $cm^3\ mol^{-1}$	$\Delta\chi_{T1}$, $cm^3\ mol^{-1}$	τ_1, s	α_1	$\Delta\chi_{T2}$, $cm^3\ mol^{-1}$	τ_2, s	α_2
0	0.086	0.950	$1.885\cdot10^{-4}$	0.066	0.670	$4.822\cdot10^{-5}$	0.202
500	0.061	1.727	$1.880\cdot10^{-3}$	0.093	–	–	–
1000	0.010	1.757	$2.000\cdot10^{-3}$	0.074	–	–	–
1500	0.009	1.744	$2.020\cdot10^{-3}$	0.071	–	–	–
2500	0.002	1.721	$1.890\cdot10^{-3}$	0.076	–	–	–
5000	0.002	1.578	$1.310\cdot10^{-3}$	0.077	–	–	–

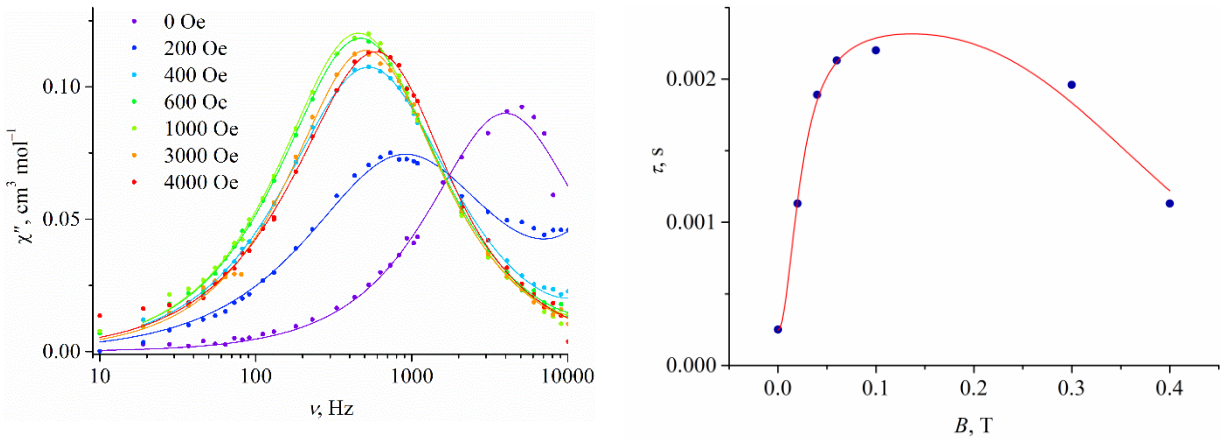

(a) (b)

Figure S18. Frequency dependences of the out-of-phase (a) ac susceptibility; (b) field dependence of the relaxation time τ for **3** at 10 K. Symbols are experimental data; solid lines indicate fits.

Table S11 Best fit parameters for **3** at 10 K (R^2 = 0.99798)

H, Oe	χ_S, cm^3 mol^{-1}	$\Delta\chi_T$, cm^3 mol^{-1}	τ, s	α
0	0.029	0.182	$3.980\cdot10^{-5}$	0.007
200	0.022	0.181	$1.799\cdot10^{-4}$	0.134
400	0.027	0.235	$3.009\cdot10^{-4}$	0.058
600	0.028	0.248	$3.391\cdot10^{-4}$	0.031
1000	0.020	0.249	$3.503\cdot10^{-4}$	0.023
3000	0.025	0.229	$3.121\cdot10^{-4}$	0.004
4000	0.027	0.219	$1.799\cdot10^{-4}$	0.074

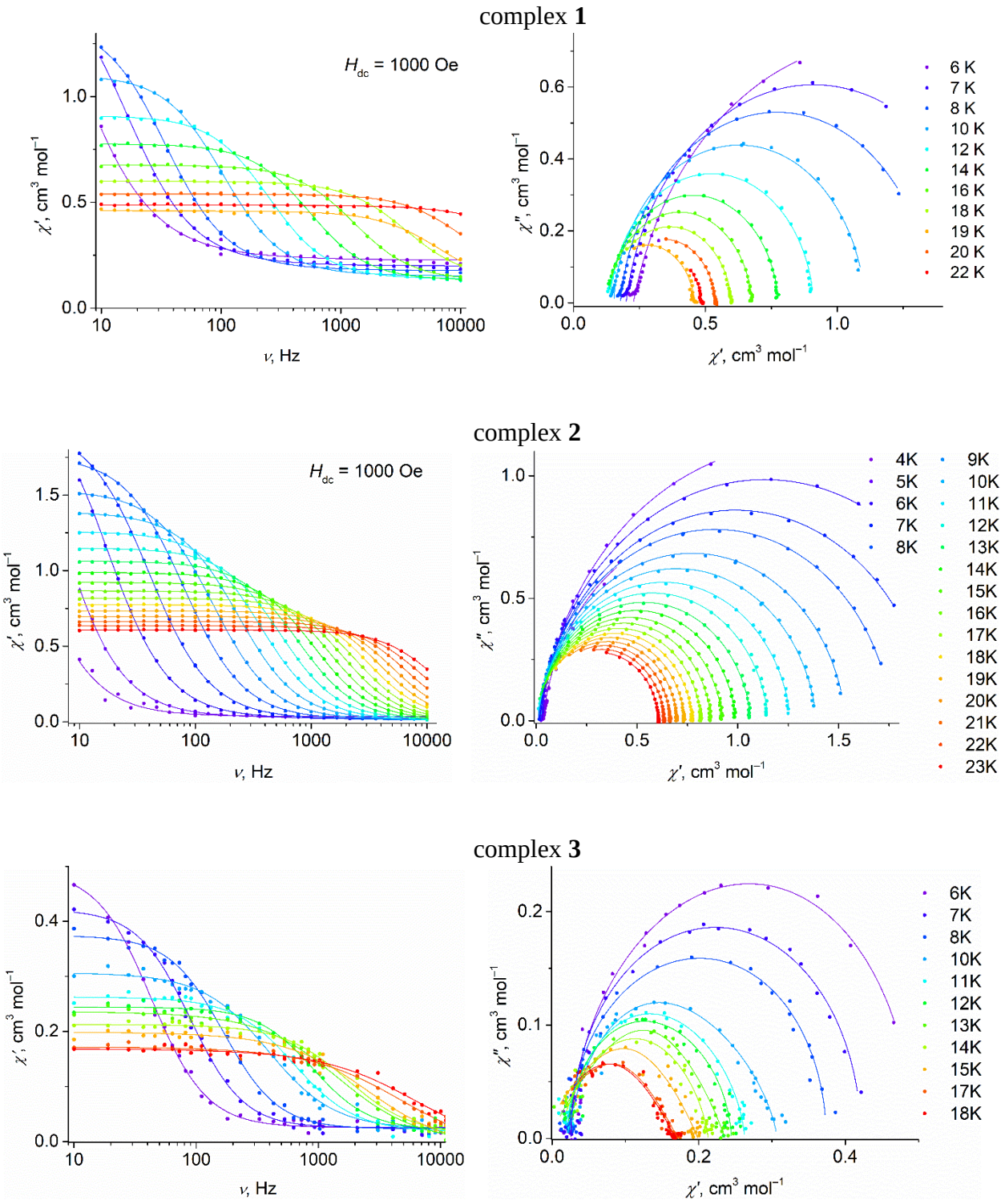

Figure S19. Frequency dependences of the in-phase ac susceptibility (left panel) and Cole−Cole plots (right panel) for complexes **1–3** at dc field 1000 Oe and stated temperatures. Dots are experimental data; solid lines indicate fit data with parameters listed in Tables S12-S14.

Table S12 Best fit parameters for **1** at dc field 1000 Oe ($R^2 = 0.99949$)

T, K	χ_S, cm^3 mol^{-1}	$\Delta\chi_T$, cm^3 mol^{-1}	τ, s	α
6	0.227	1.864	$2.677\cdot10^{-2}$	0.159
7	0.199	1.423	$9.640\cdot10^{-3}$	0.101
8	0.178	1.189	$4.640\cdot10^{-3}$	0.073
10	0.152	0.953	$1.520\cdot10^{-3}$	0.053
12	0.138	0.773	$6.367\cdot10^{-4}$	0.046
14	0.131	0.645	$2.908\cdot10^{-4}$	0.048
16	0.130	0.546	$1.238\cdot10^{-4}$	0.051
18	0.131	0.469	$4.487\cdot10^{-5}$	0.065
19	0.097	0.363	$2.359\cdot10^{-5}$	0.076
20	0.153	0.386	$1.564\cdot10^{-5}$	0.057
22	0.035	0.452	$3.079\cdot10^{-6}$	0.131

Table S13 Best fit parameters for **2** at dc field 1000 Oe ($R^2 = 0.99893$)

T, K	χ_S, cm^3 mol^{-1}	$\Delta\chi_T$, cm^3 mol^{-1}	τ, s	α
4	0.034	1.785	$3.615\cdot10^{-2}$	0.070
5	0.024	2.545	$2.393\cdot10^{-2}$	0.077
6	0.017	2.233	$9.130\cdot10^{-3}$	0.080
7	0.013	1.952	$4.010\cdot10^{-3}$	0.080
8	0.010	1.757	$2.000\cdot10^{-3}$	0.074
9	0.009	1.526	$1.110\cdot10^{-3}$	0.069
10	0.008	1.382	$6.739\cdot10^{-4}$	0.067
11	0.004	1.257	$4.372\cdot10^{-4}$	0.067
12	0.007	1.144	$2.928\cdot10^{-4}$	0.058
13	0.004	1.061	$2.067\cdot10^{-4}$	0.058
14	0.006	0.983	$1.509\cdot10^{-4}$	0.055
15	0.006	0.917	$1.126\cdot10^{-4}$	0.053
16	0.007	0.859	$8.570\cdot10^{-5}$	0.047
17	0.007	0.811	$6.624\cdot10^{-5}$	0.046
18	0.011	0.763	$5.178\cdot10^{-5}$	0.042
19	0.010	0.724	$4.009\cdot10^{-5}$	0.039
20	0.014	0.683	$3.149\cdot10^{-5}$	0.034
21	0.015	0.649	$2.421\cdot10^{-5}$	0.035
22	0.019	0.616	$1.855\cdot10^{-5}$	0.034
23	0.021	0.587	$1.402\cdot10^{-5}$	0.032

Table S14 Best fit parameters for **3** at dc field 1000 Oe (R^2 = 0.99892)

T, K	χ_S, cm^3 mol^{-1}	$\Delta\chi_T$, cm^3 mol^{-1}	τ, s	α
6	0.026	0.454	$0.386\cdot10^{-2}$	0.007
7	0.025	0.375	$0.178\cdot10^{-2}$	0.005
8	0.022	0.327	$9.649\cdot10^{-4}$	0.020
10	0.020	0.249	$3.503\cdot10^{-4}$	0.023
11	0.017	0.225	$2.356\cdot10^{-4}$	0.017
12	0.020	0.209	$1.656\cdot10^{-4}$	0.007
13	0.015	0.194	$1.226\cdot10^{-4}$	0.011
14	0.011	0.181	$9.235\cdot10^{-5}$	0.019
15	0.013	0.166	$6.687\cdot10^{-5}$	0.030
17	0.012	0.143	$3.662\cdot10^{-5}$	0.057
18	0.011	0.141	$2.707\cdot10^{-5}$	0.091

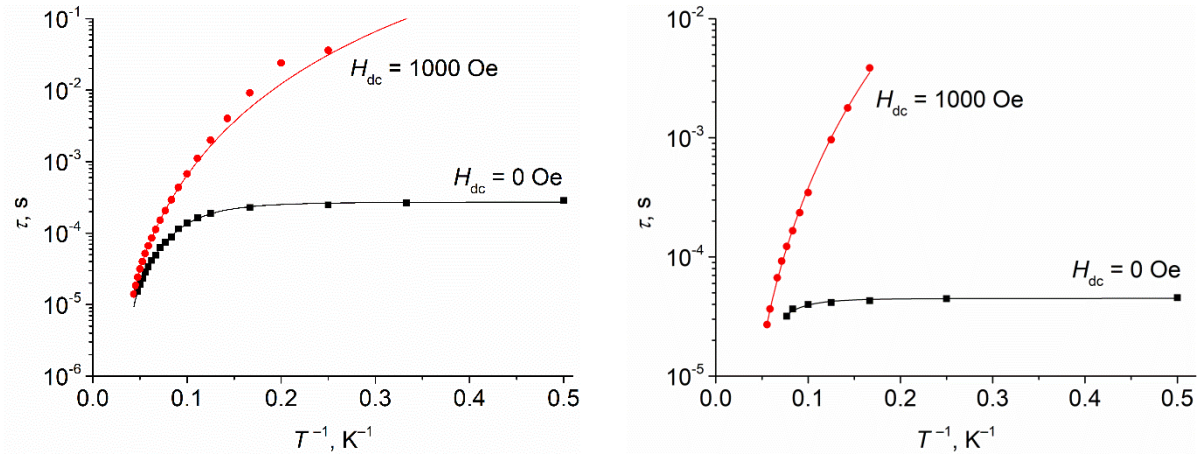

Figure S20. The inverse temperature dependences of the relaxation time τ for **2** (a) and **3** (b) at zero dc field (black lines) and 1000 Oe (red lines).

Table S15 The *ab initio* computed energy levels (cm^{-1}) with g-tensors of the eight lowest KDs for two crystallographic non-equivalent complexes in **1** and **2**

	1a				**1b**			
KD	*Energy*	g_x	g_y	g_z	*Energy*	g_x	g_y	g_z
1	0.0	0.026	0.073	19.610	0.0	0.029	0.076	19.602
2	162.9	1.834	2.844	12.024	162.8	2.136	2.402	12.551
3	191.5	1.882	2.618	15.032	197.7	1.215	4.217	13.929
4	227.8	0.115	1.794	6.850	229.7	1.225	1.900	5.615
5	387.5	1.949	4.848	11.858	390.6	1.853	4.870	11.836
6	420.7	1.022	3.420	15.062	427.2	1.125	3.415	15.216
7	510.9	2.289	2.796	12.286	514.2	2.296	2.575	12.226
8	650.1	0.314	0.816	17.496	651.5	0.321	0.872	17.436

	2a				2b			
KD	*Energy*	g_x	g_y	g_z	*Energy*	g_x	g_y	g_z
1	0.0	0.030	0.064	19.691	0.0	0.018	0.040	19.720
2	187.8	1.125	2.514	14.534	192.7	0.968	2.373	13.849
3	241.8	0.824	1.087	12.646	244.8	0.343	1.052	11.605
4	282.3	0.067	1.262	13.344	289.7	0.240	1.090	15.238
5	395.9	2.181	3.458	14.455	404.5	1.999	3.441	13.878
6	488.3	9.407	5.338	0.727	491.9	9.411	5.381	0.687
7	586.8	2.384	5.431	10.339	579.4	2.427	5.925	9.911
8	721.1	0.331	1.257	17.175	712.3	0.310	1.198	17.227

Table S16 SINGLE_ANISO computed wave function decomposition analysis for lowest KDs of Dy(III) ions for two crystallographic non-equivalent complexes in **1** and **2**. It is shown only main (> 10%) contributions

	wave function decomposition analysis (main (> 10%) contributions)	
KD	**1a**	**1b**
1	0.948 |±15/2›	0.950 |±15/2›
2	0.409 |±13/2› + 0.327 |±9/2› + 0.195 |±5/2›	0.427 |±13/2› + 0.351 |±9/2› + 0.173 |±5/2›
3	0.301 |±7/2› + 0.245 |±1/2› + 0.149 |±3/2›	0.350 |±7/2› + 0.227 |±1/2› + 0.128|±3/2›+ 0.116|±11/2›
4	0.383 |±11/2› + 0.212 |±7/2› + 0.149 |±3/2›	0.345 |±11/2› + 0.188 |±3/2› + 0.161 |±7/2› + 0.106 |±5/2›
5	0.454 |±13/2› + 0.313 |±9/2› + 0.123 |±5/2›	0.461 |±13/2› + 0.309 |±9/2› + 0.129 |±5/2›
6	0.290 |±11/2› + 0.273 |±7/2› + 0.189 |±5/2› + 0.163 |±9/2›	0.296 |±11/2› + 0.287 |±7/2› + 0.179 |±5/2› + 0.164 |±9/2›
7	0.347 |±3/2› + 0.287 |±5/2› + 0.155 |±11/2› + 0.143 |±7/2›	0.352 |±3/2› + 0.289 |±5/2› + 0.153 |±11/2› + 0.137 |±7/2›
8	0.636 |±1/2› + 0.262 |±3/2›	0.637 |±1/2› + 0.260 |±3/2›

	wave function decomposition analysis (main (> 10%) contributions)	
KD	**2a**	**2b**
1	0.962 |±15/2›	0.966 |±15/2›
2	0.499 |±13/2› + 0.346 |±9/2›	0.508 |±13/2› + 0.366 |±9/2› + 0.103|±5/2›
3	0.425 |±7/2› + 0.292 |±11/2› + 0.112|±5/2›	0.466 |±7/2› + 0.384 |±11/2›
4	0.284 |±3/2› + 0.201 |±1/2› +0.199 |±11/2› + 0.175 |±5/2›	0.313 |±3/2› + 0.228 |±1/2› +0.225 |±5/2› + 0.146 |±11/2›
5	0.355 |±13/2› + 0.321 |±9/2› + 0.138 |±7/2›	0.387 |±13/2› + 0.334 |±9/2› + 0.108 |±7/2›
6	0.254 |±5/2› + 0.202 |±11/2› + 0.180 |±7/2›+ 0.123 |±9/2›	0.231 |±5/2› + 0.227 |±11/2› + 0.224 |±7/2›+ 0.106 |±9/2›
7	0.316 |±3/2› + 0.251|±5/2› + 0.157 |±7/2› + 0.147 |±11/2›	0.319 |±3/2› + 0.270|±5/2› + 0.146 |±11/2› + 0.141 |±7/2› + 0.101 |±9/2›
8	0.611 |±1/2› + 0.259 |±3/2›	0.634 |±1/2› + 0.256 |±3/2›

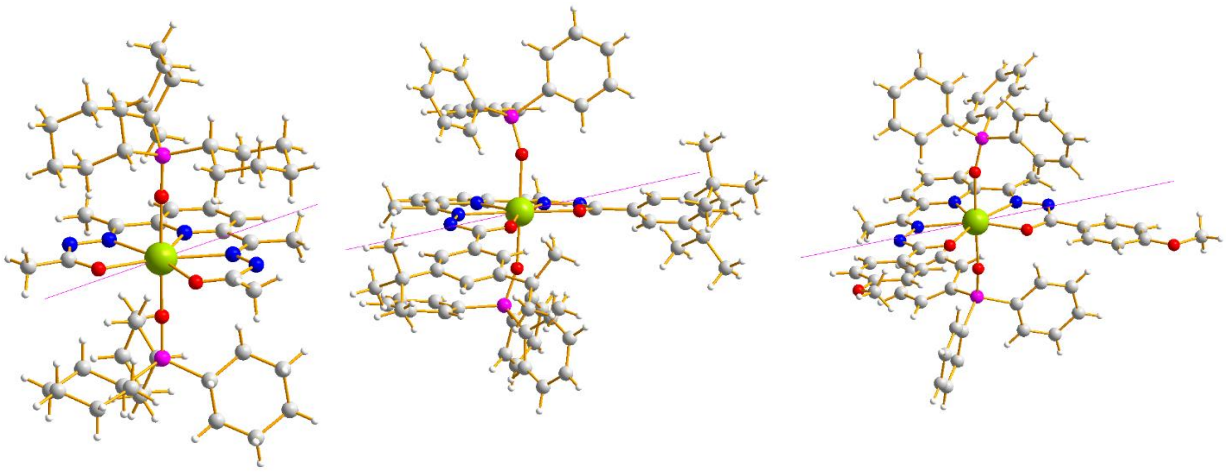

(a) (b) (c)

Figure S21. The molecular structures of **1** (a), **2** (b) and **3** (c) together with the easy axes (magenta) of ground KD obtained within the *ab initio* SA-CASSCF/RASSI-SO/SINGLE_ANISO calculation. Color code: green = Dy, magenta = P, red = O, blue = N, gray = C, white = H.

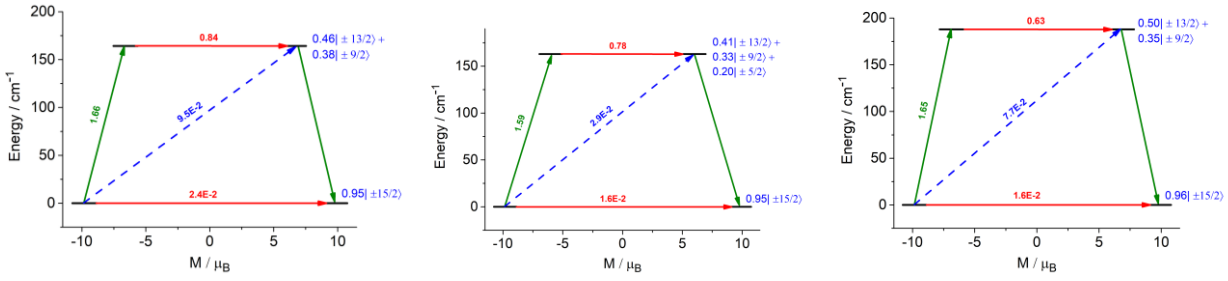

Figure S22. Computed possible magnetization relaxation pathways for **1** (a), **2** (b) and **3** (c). The red arrows show the QTM and TA-QTM via ground and higher excited KD, respectively. The blue arrow shows the Orbach process for the relaxation. The green arrows show the mechanism of magnetic relaxation.

Table S17 The *ab initio* computed CF parameter of complexes **1-3**

k	q	B_k^q		
		1	**2**	**3**
	-2	0.153E+01	-0.258E+00	-0.125E+01
	-1	-0.861E+00	0.320E-01	0.757E+00
2	0	**-0.498E+01**	**-0.255E+01**	**-0.553E+01**
	+1	0.125E+00	0.209E+01	-0.301E+01
	+2	0.286E+00	-0.291E+00	0.289E+00
	-4	-0.259E-01	0.240E-03	-0.848E-01
	-3	-0.432E-03	-0.612E-02	-0.518E-01
	-2	-0.329E+00	-0.400E-03	0.722E-01
	-1	-0.102E-03	-0.722E-02	-0.425E-01
4	0	-0.161E-01	-0.226E-02	-0.153E-01
	+1	0.259E-02	-0.830E-02	0.777E-02
	+2	-0.282E-01	0.478E-01	0.316E+00
	+3	0.150E-01	0.122E-01	0.505E-02
	+4	0.266E+00	-0.431E-01	-0.244E+00
	-6	0.158E-02	0.859E-05	0.259E-02
	-5	-0.318E-03	-0.102E-04	0.594E-03
	-4	0.188E-03	0.743E-05	0.349E-03
	-3	0.474E-03	0.972E-04	0.277E-02
	-2	0.990E-02	0.325E-04	-0.907E-03
	-1	-0.809E-03	0.197E-03	0.488E-02
6	0	-0.136E-02	-0.570E-04	-0.133E-02
	+1	-0.109E-02	-0.544E-04	0.407E-03
	+2	0.620E-03	-0.392E-03	-0.981E-02
	+3	-0.139E-02	0.478E-04	-0.241E-02
	+4	0.924E-03	-0.180E-04	-0.915E-03
	+5	0.243E-03	-0.209E-03	0.271E-02
	+6	0.738E-03	0.116E-03	0.617E-03